# Time-of-Flight Based Calibration of an Ultrasonic Computed Tomography System

*Adam FILIPÍK*[1], *Jiří JAN*[1], *Igor PETERLÍK*[2]

[1]Dept. of Biomedical Engineering, FEEC, Brno University of Technology - Czech Republic
[2]Faculty of Informatics, Masaryk University, Brno - Czech Republic

filipik@phd.feec.vutbr.cz, jan@feec.vutbr.cz, peterlik@ics.muni.cz

**Abstract.** *The paper presents a novel method for calibration of measuring geometry and of individual signal delays of transducers in ultrasonic computed tomography (USCT) systems via computational processing of multiple time-of-flight measurements of ultrasonic (US) impulses. The positions and time-delay parameters of thousands of ultrasonic transducers inside the USCT tank are calibrated by this approach with a high precision required for the tomographic reconstruction; such accuracy cannot be provided by any other known method. Although utilising similar basic principles as the global positioning system (GPS), the method is importantly generalised in treating all transducer parameters as the to-be calibrated (floating) unknowns, without any a-priori known positions and delays. The calibration is formulated as a non-linear least-squares problem, minimizing the differences between the calculated and measured time-of-arrivals of ultrasonic pulses. The paper provides detailed derivation of the method, and compares two implemented approaches (earlier calibration of individual transducers with the new approach calibrating rigid transducer arrays) via detailed simulations, aimed at testing the convergence properties and noise robustness of both approaches. Calibration using real US signals is described and, as an illustration of the utility of the presented method, a comparison is shown of two image reconstructions using the tomographic US data from a concrete experimental USCT system measuring a 3D phantom, without and after the calibration.*

## Keywords

Ultrasonic computed tomography, ultrasonic transmission tomography, calibration of sensors, nonlinear optimisation, time-of-flight measurements

## 1. Introduction

Ultrasonic Computed Tomography (USCT) is an imaging modality currently still under research, which is primarily aimed at breast cancer diagnosis. The imaged object is placed in a tank filled with water as a coupling medium, and surrounded with several thousands of ultrasonic (US) transducers. These transducers are used for either transmitting (emitters) or receiving (receivers) of ultrasonic pulses. The recorded individual signals, so called A-scans (Fig. 2), can be used for reconstruction of tomographic images of the object [1], [2], [3], based on spatial distribution of the US attenuation coefficient.

A 3D USCT system is currently being developed at Forschungszentrum Karlsruhe (KIT), Germany [1]. The system Model I (Fig. 1) consists of 384 emitters and 1536 receivers mounted on 48 exchangeable transducer array systems (TAS). The cylinder which holds the TASes can be rotated in 6 steps to achieve a total of 11,520 transducer positions, producing approximately 3.5 million A-scans per case. The transducers' mean frequency is 2.7 MHz and the A-scan signals are sampled at 10 MHz. A complete scan of an object thus produces about 20 GB of data.

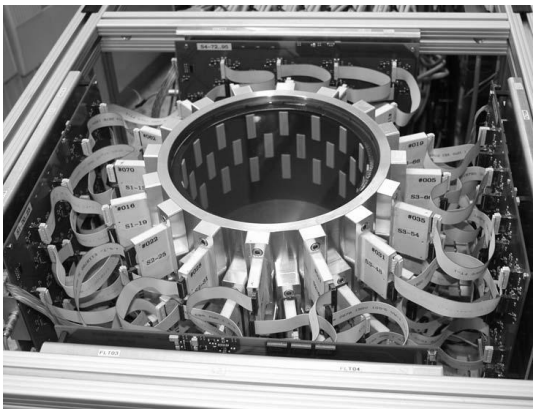

**Fig. 1.** Overview of the 3D USCT system model I in Forschungszentrum Karlsruhe – the cylindrical tank with 48 mounted transducer array systems.

The algorithms reconstructing the 3D image (i.e. local attenuation) data of tomographic images from the US measurements crucially require knowing the positions of all transducers accurately with the maximum error of the order of a fraction of the used US wavelength. Although an estimate of the positions can be made based on the dimensions of the TASes and geometry of the cylinder to which they are fixed, this is by far not sufficiently precise, as would not be also any mechanical measurement, even disregarding its complexity. With respect to the number of transducers and

their spatial distribution in the system, it is infeasible to measure the distances between them manually. But even small positioning errors (in the range of tenths of millimeters) can lead to significant degradation of the reconstructed 3D image data. Therefore, a new principle of the geometrical calibration had to be designed, which – if possible – should also enable calibration of other unknown and needed quantities: differing delays of US signals in the individual transducers.

The presented auto-calibration method, which utilizes only the internal ultrasonic signals produced by the system, can solve both calibration problems simultaneously. The technique is based on similar though generalised principles as the GPS navigation. A novelty is in considering all positions of the transducers unknown, thus not requiring the reference coordinate system as in GPS, where the orbits of the satellites (e.g. instant transmitter positions) are very accurately known. In contrast, such a positioning device is not needed in our approach, and all positions and time delays (both of the emitters and receivers) constitute the unknown variables to be determined. For the calibration, the standard internal ultrasonic signals and particularly from them derived times-of-arrivals (see below for definition) of individual ultrasonic pulses are used for triangulation. The triangulation is formulated as an iterative minimization problem, where the to-be-minimized quantity is the sum of squares of differences between the measured pulse arrival times and those estimated by the presented algorithm based on the instantaneous parameter vector.

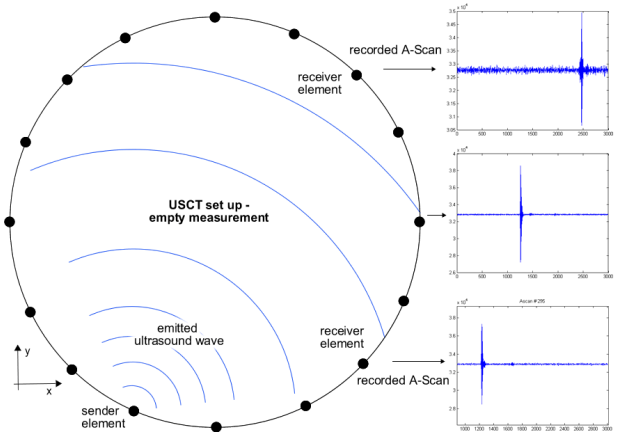


**Fig. 2.** The USCT system (simplified schematic - view from the top).

The a-priori unknown minimization parameters are the sought thousands of positions and individual time-delays of all the transducers. The formulation of the method and problems of numerical solution of the respective large systems of nonlinear equations are treated in detail together with in-depth simulations showing a good convergence stability and high robustness with respect to measurement noise. Particularly, the newer approach based on transducer arrays (TASes) instead on individual transducers turned excellent in both respects.

Calibration of such extensive measuring systems is a need in different applications; however none of the published calibration solutions was applicable to our problem. A similar situation can be seen in the calibration of an underwater ultrasound imaging system [4]. Here, the authors relied on the presence of a high precision positioning device with an attached hydrophone (serving as the emitter). The knowledge of the hydrophone positions provides a reference coordinate system to the calibration, just like in the GPS; however, such coordinate frame is not available in our case.

The presented calibration method overcomes also a problem, which is present in another calibration approach, frequently used for microphone array systems – multidimensional scaling (MDE) [5]. MDE requires all emitter-to-emitter and receiver-to-receiver distances to be measured ahead. The issue can be partially dealt with by identifying a set of basis nodes, where all inter-node distances can be measured [6]. But for systems (such as the Karlsruhe USCT), consisting of transducers, which cannot change the functional mode (each transducer is built exclusively as either an emitter or a receiver), this is infeasible. Thus the presented calibration approach is – to the authors' knowledge – the only usable option.

The paper formulates the method particularly for the concrete experimental USCT system; it should however be stressed that the method is generic and may be used for structurally similar, though physically very different problems as well. Following the project progression, some of the related gradually improving preliminary results were briefly presented and discussed at conferences [7] and [8]. This paper formulates the method in its advanced form, with details on formulation and computational aspects; presenting, besides novelties like finalising the TAS-based approach, the detailed mathematical derivation and the respective numerical approach and analysis, and describes the respective simulation methods and results. The simulation has been the only way how to verify the functionality and precision of the method, as direct physical distance measurements that would reveal the ground truth on the experimental system geometry with the required accuracy are practically infeasible; similarly, it is unrealistic to measure thousands of the individual transducer delays.

Nevertheless, the paper is concluded with demonstration of using real US signals for calibration of the concrete USCT system, and an obvious improvement in the magnitude and statistics of errors in the measurements is demonstrated when they are corrected using the calibration results. Finally, a result proving the usefulness of the calibration when used for the concrete experimental Karlsruhe USCT system is shown: based on the real US measurement set of a known 3D phantom, two reconstructions of the tomographic image data were provided, with and without compensating for the real geometry and delays of measurement, as follows from the calibration. As will be shown, the reconstruction based on calibrated data is clearly superior to that using the data without calibration. Although it is only an indirect

check, it represents an important indication of both the correctness and importance of the presented method. Regular practical use of the calibration procedure at the experimental system, providing also opportunity for its thorough evaluation, is intended in frame of the continuing research.

The paper is organized as follows: in the second chapter, the principle of the method is formulated and its two alternatives – individual-transducer approach and transducer-array approach are presented. The last section here deals with the problem of absent reference coordinate system; this is overcome by means of so-called anchoring. The third chapter is devoted to numerical formulation of the respective nonlinear optimisation problem and analyses the convergence of the method and its sensitivity to measurement noise by simulation. The fourth chapter describes the calibration based on realistic experimental data, and the application of the obtained accurate geometry and delay set of the system during the image reconstruction procedure based on concrete tomographic data. The conclusion then summarizes the most important points.

# 2. Calibration Methods

For the USCT calibration, a so-called empty measurement has to be made. In such a measurement, the tank is filled only with water. Each emitter is individually excited to produce an ultrasonic pulse wave, which travels through the water and reaches all receiving transducers. Each of the receivers records an A-scan signal (Fig. 2). The complete measurement consists of consecutively firing all emitters (one emitter at a time).

In each A-scan one or more pulses can be detected. The first one corresponds to the direct path of the ultrasound wave from the emitter to the receiver, whereas later pulses correspond to reflection paths from the tank walls or the water surface.

The calibration method calculates the transducer positions and time-delays introduced by electronics processing the signals on both the transmission and reception sides. The calculations are based on *time-of-arrival* (TOA) measurements of the direct pulse for each available emitter-receiver combination.

The next two sections describe the calibration method mathematically. The definition of the TOA is an important aspect, which has a great effect on the calibration accuracy, as will be shown below. In the first section, the TOAs are defined conventionally (as in GPS) as functions of the individual transducer positions. In the second section, we take advantage of the fact that the transducers surrounding the USCT tank are grouped into transducer array systems (TAS) within which the mutual positions of the transducers are known. The TOAs are then defined as functions of positions and orientations of the whole TASes.

## 2.1 The Individual Transducer Element Approach

Let us first introduce some necessary notation: Let $S = \{s_i, i = 1...M\}$ and $R = \{r_i, i = 1...N\}$ be two disjoint sets of the active emitters and receivers respectively. Further, let $P = \{(s,r)_k, k = 1...Q\}$ be a set of pairs $(s,r), s \in S, r \in R$ such that for each pair $(s,r) \in P$ we can detect the direct pulse in the corresponding A-scan and thus obtain a *measured time-of-arrival* value $MTOA_{sr}$.

Next let $\mathbf{x}_s = [x_s, y_s, z_s, \tau_s]$ and $\mathbf{x}_r = [x_r, y_r, z_r, \tau_r]$ be the vectors of the unknown emitter and receiver position coordinates and time-delays. We can now define the *computed time-of-arrival* $CTOA$ as a function dependent on the individual transducer element parameters:

$$CTOA_{sr}(\mathbf{x}_s, \mathbf{x}_r) = \frac{\sqrt{(x_s - x_r)^2 + (y_s - y_r)^2 + (z_s - z_r)^2}}{v} + \tau_s + \tau_r \quad (1)$$

where $v$ is the sound velocity.

The above equation is very similar to the so-called pseudorange equation used in GPS [9], where the time delay components are analogical to the satellites' and receivers' clocks offsets. There is a major difference, though, in the fact that in the USCT, neither the emitter nor the receiver positions and delays are assumed to be known. The only known parameter is the speed of sound in water $v$, which (in a controlled environment) can be very accurately calculated if the temperature is known [10].

Taking the emitter-receiver pairs from the set $P$, we have two comparable vectors — $\mathbf{CTOA}_P = [CTOA_{s,r}]$ as the vector of the computed time-of-arrival values for all the emitter–receiver pairs $(s,r) \in P$ and $\mathbf{MTOA}_P = [MTOA_{s,r}]$ as the vector of the experimentally measured values of time-of-arrival. The task can be now formulated as follows: *Find the vector* $\mathbf{x} = [\mathbf{x}_s, \mathbf{x}_r], (s,r) \in P$ *of unknown positions and delay parameters of all the emitters in S and receivers in R such that the normed difference between* $\mathbf{CTOA}_P$ *and* $\mathbf{MTOA}_P$ *is minimized.*

In other words, minimize the residual $F_P$:

$$\begin{aligned} minF_P(\mathbf{x}) &= \min_x \left\{ \frac{1}{2} ||\mathbf{CTOA}_P - \mathbf{MTOA}_P||^2 \right\} \\ &= \min_x \left\{ \frac{1}{2} \sum_{(s,r)\in P} (CTOA_{sr} - MTOA_{sr})^2 \right\} \end{aligned} \quad (2)$$

where the minimization runs in the vector space of unknown $\mathbf{x}$ which influences $\mathbf{CTOA}_P$.

Apparently, the task can be regarded as a non-linear least-squares problem, where the functional $F_P$ depends on $4M + 4N$ variables, where $M = |S|$ is number of emitters, $N = |R|$ is number of receivers. Therefore, we can apply the Gauss-Newton iteration, which minimizes the functional $F$ iteratively solving in each step a linearized system

$$\mathbf{J}(\mathbf{x}^k)^T\mathbf{J}(\mathbf{x}^k)\Delta\mathbf{x}^k = -\mathbf{J}(\mathbf{x}^k)^T\mathbf{f}(\mathbf{x}^k) \tag{3}$$

where $k$ is the iteration number, $\mathbf{J}(\mathbf{x}^k)$ is the Jacobian matrix of the functional $F$ at $\mathbf{x}^k$, $\mathbf{f}^k$ is the actual value of the residual, and $\Delta\mathbf{x}^k$ is the correction vector used for calculation of the new estimate of $\mathbf{x}$:

$$\mathbf{x}^{k+1} = \mathbf{x}^k + \Delta\mathbf{x}^k. \tag{4}$$

The initial value of $\mathbf{CTOA}_P^0$ is then computed using the initial estimates of the position and delay parameters determined from the roughly known physical dimensions of the setup.

To enable using the Gauss-Newton method, we need to formulate the vector $\mathbf{f}^k$ of residuals

$$\mathbf{f}_P^k = \left[f_{sr}^k\right] = \mathbf{MTOA}_P - \mathbf{CTOA}_P^k \tag{5}$$

and the matrix $\mathbf{J}^k$, the elements of which are the partial derivatives of the residuals:

$$\mathbf{J}^k = (j_{i,j}^k) = \left(\frac{\partial \mathbf{f}_i^k}{\partial \mathbf{x}_j}\right) \tag{6}$$

where the index $i = 1\ldots MN$ spans the number of emitter-receiver pairs, and the index $j = 1\ldots 4M+4N$ spans the number of estimated parameters. One row of the matrix contains the partial derivatives of a particular emitter-receiver pair residual $f_{sr}$ with respect to all of the emitter and receiver parameters in $\mathbf{x}$. However, the only nonzero partial derivatives of $f_{sr}$ are the ones with respect to the $x_s, y_s, z_s, \tau_s$ and $x_r, y_r, z_r, \tau_r$ parameters of the corresponding emitter-receiver pair,

$$\begin{array}{ll}
\frac{\partial f_{sr}^k}{\partial x_s} = \frac{x_s^k - x_r^k}{v d_{sr}^k}, & \frac{\partial f_{sr}^k}{\partial y_s} = \frac{y_s^k - y_r^k}{v d_{sr}^k}, \\
\frac{\partial f_{sr}^k}{\partial x_r} = \frac{-(x_s^k - x_r^k)}{v d_{sr}^k}, & \frac{\partial f_{sr}^k}{\partial y_r} = \frac{-(y_s^k - y_r^k)}{v d_{sr}^k}, \\
\frac{\partial f_{sr}^k}{\partial z_s} = \frac{z_s^k - z_r^k}{v d_{sr}^k}, & \frac{\partial f_{sr}^k}{\partial \tau_s} = 1, \\
\frac{\partial f_{sr}^k}{\partial z_r} = \frac{-(z_s^k - z_r^k)}{v d_{sr}^k}, & \frac{\partial f_{sr}^k}{\partial \tau_r} = 1
\end{array} \tag{7}$$

where the emitter-receiver distance estimate $d_{sr}^k = \sqrt{(x_s^k - x_r^k)^2 + (y_s^k - y_r^k)^{2+(z_s^k - z_r^k)^2}}$. Summarizing, the $k$-th equation in the equation system (3) has the form

$$\frac{x_s^k - x_r^k}{v d_{sr}^k}\Delta x_s^k + \frac{y_s^k - y_r^k}{v d_{sr}^k}\Delta y_s^k + \frac{z_s^k - z_r^k}{v d_{sr}^k}\Delta z_s^k + \Delta\tau_s^k - \frac{x_s^k - x_r^k}{v d_{sr}^k}\Delta x_r^k - \frac{y_s^k - y_r^k}{v d_{sr}^k}\Delta y_r^k - \frac{z_s^k - z_r^k}{v d_{sr}^k}\Delta z_r^k + \Delta\tau_r^k = MTOA_{sr} - CTOA_{sr}^k. \tag{8}$$

To cope with the presence of noise in measurements, we require the number of measured time-of-arrival values $Q = |P| = MN$ to be significantly larger than the number of unknown variables $V = 4M + 4N$, i.e. $MN \gg 4M + 4N$. This requirement is more than accomplished in the current USCT set up as $Q = 384 \cdot 1536 = 589,824$ and $V = 4 \cdot 384 + 4 \cdot 1536 = 7,680$, so that the system (3) is overdetermined.

An alternative to the Gauss-Newton method might be the Levenberg-Marquardt method [11], which is however more suited for strong nonlinearities in the minimization function.

## 2.2 The Transducer Array System Approach

In order to achieve greater accuracy and make the calibration less prone to TOA detection errors, we can use additional information about positions of the transducers within a transducer array system (TAS). Because each TAS is manufactured in the same way (including a precise sawing technique, [3]) we can assume that all transducer elements in one TAS lie on a plane in known positions. We can reformulate the calibration problem to involve the *positions and orientations of TASes* rather than the positions of the individual transducer elements.

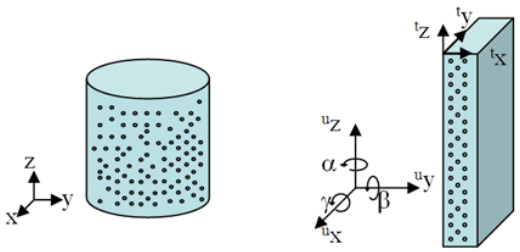


**Fig. 3.** In the ITE approach we seek to find the positions of individual transducer elements on the USCT cylinder (left), whereas in the TAS approach we seek the positions and orientations of the TAS casings (right).

To express the relationship of transducer positions in the USCT (world) coordinate system $\{^u x, ^u y, ^u z\}$ and the TAS coordinate system $\{^t x, ^t y, ^t z\}$, the $x$-$y$-$z$ fixed angle parameterization scheme, depicted in [12], was adopted. The coordinate transformation is done by first rotating the TAS by $g$ around the $^u x$ axis, then by $b$ around the $^u y$ axis, and last by $a$ around the $^u z$ axis. Finally the whole TAS is translated by $\{x, y, z\}$. Thus the transformation of each point from the TAS coordinate system to the USCT coordinate system can be expressed as a multiplication of a position vector in TAS by a homogeneous rotation-translation matrix (9) (see next page).

The relations in (9) can be used to redefine the computed time-of-arrival $CTOA_{sr}$ in (1) as the function (10), where the subscripts "st" and "rt" denote parameters of emitter and receiver TASes respectively, all in the USCT coordinate system. The subscripts "se" and "re" denote emitter and receiver element parameters in the TAS coordinate systems.

As in the ITE approach, we have vectors of the computed and measured time-of-arrival values for each emitter-receiver pair $\mathbf{CTOA}_P$ and $\mathbf{MTOA}_P$, except that now, $\mathbf{CTOA}_P = \mathbf{CTOA}_P(\mathbf{x})$ is a function of the newly defined vector $\mathbf{x} = [\mathbf{x}_t, \tau_s, \tau_r]$ of all the TAS parameters $\mathbf{x}_T = [x_t, y_t, z_t, \alpha_t, \beta_t, \gamma_t], t \in T$ and all the emitter and receiver time delays $\tau_S = [\tau_s], s \in S$ and $\tau_R = [\tau_r], r \in R$. We can now again define the calibration problem as: *Find the vector* $\mathbf{x}$ *such that*

*the norm of difference between* $\mathbf{CTOA}_P$ *and* $\mathbf{MTOA}_P$ *is minimized.* The definition of the residual (2) remains the same.

Because $CTOA_{sr}$ in (10) is a nonlinear function of the unknown TAS parameters, the Gauss-Newton method (3) and (4) is again used to solve the nonlinear system of equations. While the definition of the residual (5) remains the same as in the ITE approach, the elements of the Jacobian matrix (6) will be different than in (7). The only non-zero elements of the Jacobian in one row (corresponding to a particular emitter-receiver pair) are the partial derivatives of the residual $f_{sr}$ with respect to the parameters of the corresponding emitter and receiver TASes, and the emitter- and receiver-element time-delay parameters (11) and (12), where the $D_x^k, D_y^k, D_z^k, R^k$ are defined in (13).

$$\begin{bmatrix} {}^{u}x \\ {}^{u}y \\ {}^{u}z \\ 1 \end{bmatrix} = \begin{bmatrix} \cos(\alpha)\cos(\beta) & \cos(\alpha)\sin(\beta)\sin(\gamma)-\sin(\alpha)\cos(\gamma) & \cos(\alpha)\sin(\beta)\cos(\gamma)+\sin(\alpha)\sin(\gamma) & x \\ \sin(\alpha)\cos(\beta) & \sin(\alpha)\sin(\beta)\sin(\gamma)+\cos(\alpha)\cos(\gamma) & \sin(\alpha)\sin(\beta)\cos(\gamma)-\cos(\alpha)\sin(\gamma) & y \\ -\sin(\beta) & \cos(\beta)\sin(\gamma) & \cos(\beta)\cos(\gamma) & z \\ 0 & 0 & 0 & 1 \end{bmatrix} \cdot \begin{bmatrix} {}^{t}x \\ {}^{t}y \\ {}^{t}z \\ 1 \end{bmatrix}, \tag{9}$$

$$\begin{aligned} CTOA_{sr} &= \sqrt{d_x^2+d_y^2+d_z^2}/v+\tau_s+\tau_r, \\ d_x &= \cos(\alpha_{st})\cos(\beta_{st})x_{se}+(\cos(\alpha_{st})\sin(\beta_{st})\cos(\gamma_{st})+\sin(\alpha_{st})\sin(\gamma_{st}))z_{se}+x_{st}-\cos(\alpha_{rt})\cos(\beta_{rt})x_{re} \\ &\quad -(\cos(\alpha_{rt})\sin(\beta_{rt})\cos(\gamma_{rt})+\sin(\alpha_{rt})\sin(\gamma_{rt}))z_{re}-x_{rt}, \\ d_y &= \sin(\alpha_{st})\cos(\beta_{st})x_{se}+(\sin(\alpha_{st})\sin(\beta_{st})\cos(\gamma_{st})-\cos(\alpha_{st})\sin(\gamma_{st}))z_{se}+y_{st}-\sin(\alpha_{rt})\cos(\beta_{rt})x_{re} \\ &\quad -(\sin(\alpha_{rt})\sin(\beta_{rt})\cos(\gamma_{rt})-\cos(\alpha_{rt})\sin(\gamma_{rt}))z_{re}-y_{rt}, \\ d_z &= -\sin(\beta_{st})x_{se}+\cos(\alpha_{st})\cos(\gamma_{st})z_{se}+z_{st}+\sin(\beta_{rt})x_{re}-\cos(\beta_{rt})\cos(\gamma_{rt})z_{re}-z_{rt}, \end{aligned} \tag{10}$$

$$\begin{aligned} \frac{\partial f_{sr}^k}{\partial \alpha_{st}} &= (D_x^k(-\sin(\alpha_{st}^k)\cos(\beta_{st}^k)x_{se}+(-\sin(\alpha_{st}^k)\sin(\beta_{st}^k)\cos(\gamma_{st}^k)+\cos(\alpha_{st}^k)\sin(\gamma_{st}^k))z_{se}) \\ &\quad +D_y^k(\cos(\alpha_{st}^k)\cos(\beta_{st}^k)x_{se}+(\cos(\alpha_{st}^k)\sin(\beta_{st}^k)\cos(\gamma_{st}^k)+\sin(\alpha_{st}^k)\sin(\gamma_{st}^k))z_{se}))R^k v, \\ \frac{\partial f_{sr}^k}{\partial \beta_{st}} &= (D_x^k(-\cos(\alpha_{st}^k)\sin(\beta_{st}^k)x_{se}+\cos(\alpha_{st}^k)\cos(\beta_{st}^k)\cos(\gamma_{st}^k)z_{se})+D_y^k(-\sin(\alpha_{st}^k)\sin(\beta_{st}^k)x_{se} \\ &\quad +\sin(\alpha_{st}^k)\cos(\beta_{st}^k)\cos(\gamma_{st}^k)z_{se})+D_z(-\cos(\beta_{st}^k))x_{se}-\sin(\beta_{st}^k)\cos(\gamma_{st}^k)z_{se}))/R^k v, \\ \frac{\partial f_{sr}^k}{\partial \gamma_{st}} &= (D_x^k(-\cos(\alpha_{st}^k)\sin(\beta_{st}^k)\sin(\gamma_{st}^k)+\sin(\alpha_{st}^k)\cos(\gamma_{st}^k))z_{se}+D_y^k(-\sin(\alpha_{st}^k)\sin(\beta_{st}^k)\sin(\gamma_{st}^k) \\ &\quad +\cos(\alpha_{st}^k)\cos(\gamma_{st}^k))z_{se}+D_z^k\cos(\beta_{st}^k)\sin(\gamma_{st}^k)z_{se}/R^k v, \\ \frac{\partial f_{sr}^k}{\partial x_{st}} &= D_x^k/R^k v, \frac{\partial f_{sr}^k}{\partial y_{st}} = D_y^k/R^k v, \frac{\partial f_{sr}^k}{\partial z_{st}} = D_z^k/R^k v, \frac{\partial f_{sr}^k}{\partial \tau_s} = 1, \end{aligned} \tag{11}$$

$$\begin{aligned} \frac{\partial f_{sr}^k}{\partial \alpha_{rt}} &= (D_x^k(\sin(\alpha_{rt}^k)\cos(\beta_{rt}^k)x_{se}-(-\sin(\alpha_{rt}^k)\sin(\beta_{rt}^k)\cos(\gamma_{rt}^k)+\cos(\alpha_{rt}^k)\sin(\gamma_{rt}^k))z_{se}) \\ &\quad +D_y^k(-\cos(\alpha_{rt}^k)\cos(\beta_{rt}^k)x_{se}-(\cos(\alpha_{rt}^k)\sin(\beta_{rt}^k)\cos(\gamma_{rt}^k)+\sin(\alpha_{rt}^k)\sin(\gamma_{rt}^k))z_{se}))R^k v, \\ \frac{\partial f_{sr}^k}{\partial \beta_{rt}} &= (D_x^k(\cos(\alpha_{rt}^k)\sin(\beta_{rt}^k)x_{se}-\cos(\alpha_{rt}^k)\cos(\beta_{rt}^k)\cos(\gamma_{rt}^k)z_{se})+D_y^k(\sin(\alpha_{rt}^k)\sin(\beta_{rt}^k)x_{se} \\ &\quad -\sin(\alpha_{rt}^k)\cos(\beta_{rt}^k)\cos(\gamma_{rt}^k)z_{se})+D_z(\cos(\beta_{rt}^k))x_{se}+\sin(\beta_{rt}^k)\cos(\gamma_{rt}^k)z_{se}))/R^k v, \\ \frac{\partial f_{sr}^k}{\partial \gamma_{rt}} &= (-D_x^k(-\cos(\alpha_{rt}^k)\sin(\beta_{rt}^k)\sin(\gamma_{rt}^k)+\sin(\alpha_{rt}^k)\cos(\gamma_{rt}^k))z_{se}+D_y^k(-\sin(\alpha_{rt}^k)\sin(\beta_{rt}^k)\sin(\gamma_{rt}^k) \\ &\quad -\cos(\alpha_{rt}^k)\cos(\gamma_{rt}^k))z_{se}+D_z^k\cos(\beta_{rt}^k)\sin(\gamma_{rt}^k)z_{se}/R^k v, \\ \frac{\partial f_{sr}^k}{\partial x_{rt}} &= -D_x^k/R^k v, \frac{\partial f_{sr}^k}{\partial y_{rt}} = -D_y^k/R^k v, \frac{\partial f_{sr}^k}{\partial z_{rt}} = -D_z^k/R^k v, \frac{\partial f_{sr}^k}{\partial \tau_s} = 1, \end{aligned} \tag{12}$$

$$
\begin{aligned}
D_x^k &= \cos(\alpha_{rt}^k)\cos(\beta_{rt}^k)x_{se} + (\cos(\alpha_{rt}^k)\sin(\beta_{rt}^k)\cos(\gamma_{rt}^k) + \sin(\alpha_{rt}^k)\sin(\gamma_{rt}^k))z_{se} + x_{rt}^k - \cos(\alpha_{rt}^k)\cos(\beta_{rt}^k)x_{re} \\
&\quad - \cos(\alpha_{rt}^k)\sin(\beta_{rt}^k)\cos(\gamma_{rt}^k) + \sin(\alpha_{rt}^k)\sin(\gamma_{rt}^k))z_{re} - x_{re}^k, \\
D_y^k &= \sin(\alpha_{rt}^k)\cos(\beta_{rt}^k)x_{se} + (\sin(\alpha_{rt}^k)\sin(\beta_{rt}^k)\cos(\gamma_{rt}^k) - \cos(\alpha_{rt}^k)\sin(\gamma_{rt}^k))z_{se} + y_{rt}^k - \sin(\alpha_{rt}^k)\cos(\beta_{rt}^k)x_{re} \\
&\quad - (\sin(\alpha_{rt}^k)\sin(\beta_{rt}^k)\cos(\gamma_{rt}^k) - \cos(\alpha_{rt}^k)\sin(\gamma_{rt}^k))z_{re} - y^k - rt, \\
D_z^k &= -\sin(\beta_{rt}^k)x_{se} + \cos(\beta_{rt}^k)\cos(\gamma_{rt}^k)z_{se} + z_{se}^k + \sin(\beta_{rt}^k)x_{re} - \cos(\beta_{rt}^k)\cos(\gamma_{rt}^k)z_{re} - z_{rt}^k, \\
R^k &= \sqrt{(D_x^k)^2 + (D_y^k)^2 + (D_z^k)^2}.
\end{aligned} \tag{13}
$$

In each iteration of the Gauss-Newton method, these equations are used to calculate the Jacobian **J,** which is then used in (3) thus defining the linearized equation system for $\Delta\mathbf{x}$. The vector of the estimated parameters is then updated (4). After convergence, the needed positions of individual transducers can be calculated based on the calibrated TAS positions and orientations using (9).

The number of emitter-receiver pairs in the TAS approach is the same as in the ITE approach and therefore the number of equations remains unchanged. However, the number of the variables is: $V = 6U + M + N$, where $U$, $M$, $N$ are the numbers of TASes, emitters, and receivers respectively. In the current USCT set up there are 48 TASes in 3 layers (16 in each), thus $V = 6 \cdot 48 + 384 + 1536 = 2,208$. Compared to the ITE approach, the TAS approach significantly reduces the number of unknowns while maintaining the same number of equations. This means the calibration solution is much less prone to errors due to noisy data.

## 2.3 Anchoring

In order to obtain a unique solution of the nonlinear calibration problem by either of the two approaches (ITE or TAS), we have to introduce some constraints. With the calibration, we are seeking the positions and individual time-delays of the transducers based only on the time-of-flight measurements. No information is provided on the position and orientation of the USCT transducers relative to a particular coordinate system, in contrast to the GPS case, where a reference coordinate system is defined by the known positions and time-delays of the satellites.

Consequently, the USCT equation system matrix is rank deficient (the rank is always by 7 less than the full rank – one for each degree of freedom (three translational, three rotational, and one time degree) and even though the system of equations is heavily overdetermined, it has an infinite number of solutions.

To obtain a single solution, we can constrain the system of equations by introducing virtual "anchors" – reference points defining the coordinate system of the solution.

In the conceptually simpler ITE case, we can for example anchor the emitter element #1 to the origin of the coordinate system: $s_1 : \{0,0,0\}$ by setting the $x$, $y$, and $z$ coordinates of $s_1$ to zero in the initial estimate $\mathbf{x}^k$, $k = 0$. To insure that the position of $s_1$ is not altered by the least squares solution, we must add an equation, one for each coordinate, expressing the stability of the solution with respect to each error component of $s_1 : \Delta x_{s1} = 0,\ \Delta y_{s1} = 0,\ \Delta z_{s1} = 0$. This leads to adding 3 rows to the Jacobian matrix with all components equal to zero except those matching $x$, $y$ and $z$ error components of $s_1$. The corresponding residual values need to be set to zero.

The three anchors of the $s_1$ transducer constrain the three translational degrees of freedom of the coordinate system. The three rotational degrees of freedom can be constrained by anchoring other transducers, but only to the extent not constraining their mutual distances. Thus we can anchor only two out of the three coordinates of the transducer $s_2 : \{x_{const},\ y_{const},\ z\}$. This way, the distance between $s_1$ and $s_2$ can still be adjusted by solving the least squares problem. To constrain the coordinate system completely, we need to anchor the $z$ coordinate of yet another transducer $s_3 : \{x,\ y,\ z_{const}\}$.

In case of TAS approach we have more options. It is for example sufficient to anchor only one of the TASes, fixing all of its position and orientation parameters ($x$, $y$, $z$, $\alpha$, $\beta$, $\gamma$). This anchors all of the 6 spatial degrees of freedom. Alternatively, it is also possible to anchor two or more TASes with a combination of $\alpha$, $\beta$, $\gamma$, $x$, $y$, and $z$ anchors.

We face a similar problem with the variability of the time-delay parameters. Both $CTOA_{sr}$ definitions (1) and (10) (for the ITE and TAS approach respectively) contain a sum of two time delay parameters: the errors of the respective emitter delay and the respective receiver delay. This sum is inseparable: an arbitrary time constant $t_{arb}$ may be added to all emitter delays and subtracted from all receiver delays, without influencing the solution of our equation system. The system is thus still rank deficient.

We cannot proceed analogically to the previous case and anchor the delay of one transducer, for example set $\tau_{s1} = 0$, as this would introduce a systematic error. However, we can "anchor" the sum of all emitter delay errors to a constant value, e.g. zero:

$$\sum_i \Delta\tau_{s_i} = 0, \tag{14}$$

this way constraining the unlimited number of solutions to only a single one. Although we constrain the system to one solution, the solved delay values will be biased by an unknown quantity $t_{arb}$:

$$\begin{aligned} \tau_{s_i,solved} &= \tau_{s_i,true} + t_{arb}, \forall i, \\ \tau_{r_j,solved} &= \tau_{r_j,true} - t_{arb}, \forall j. \end{aligned} \tag{15}$$

The solved delay parameters (biased by $t_{arb}$) can thus reach physically impossible (negative) values. However, in any single measurement, the TOA of a pulse depends on the sum of the emitter and receiver delays, where $t_{arb}$ vanishes (15). Thus, the sum of delays of an emitter and a receiver can be recovered.

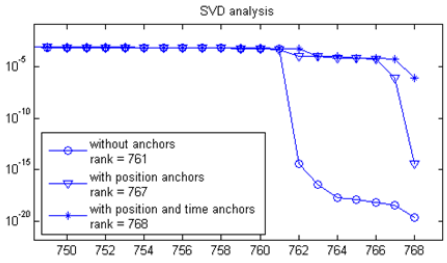


**Fig. 4.** SVD analysis of the Jacobian matrix (with 768 columns) with and without anchoring. The singular values (vertical logarithmic axis) were sorted in descending order (horizontal axis: value index); only the last few (smallest) singular values are shown. With both position and time anchoring, the matrix has a full column rank.

A simple verification of the anchoring concept can be made by singular value decomposition, calculating the rank of the equation system – the number of linearly independent equations. The rank can be estimated as the number of singular values of the system matrix, which are larger than some tolerance value (related to the machine precision) [1]. The singular values of the Jacobian matrix (6) with and without anchors are plotted in Fig. 4. We clearly see that the smallest singular values were raised significantly by the inclusion of the anchoring equations to the system – the full column rank was reached.

## 3. Numerical Simulation Analysis

In order to evaluate the method, a simulation study has been carried out based on a virtual model of the USCT system. 64 emitters and 128 receivers in 16 TASes were taken into consideration (about 1/10 of the actual numbers). This resulted in $N_{un} = (64 + 128)4 = 768$ unknown parameters (3 position coordinates and 1 delay per transducer) for the ITE approach and $N_{un}$ = (64 + 128) + 16 (3+3) = 288 unknown parameters (1 delay per transducer and 3 position and 3 orientation unknowns per TAS) for the TAS approach. The number of simulated TOA measurements was the same for both ITE and TAS approaches $N_{eq} = 64 \cdot 128 = 8192$. The simulation was carried out in Matlab. To solve the equation system (5), the QR-decomposition with pivoting (implemented in the Matlab's backslash operator) was used.

This USCT simulation was used to analyze the convergence properties and the noise sensitivity of the calibration method.

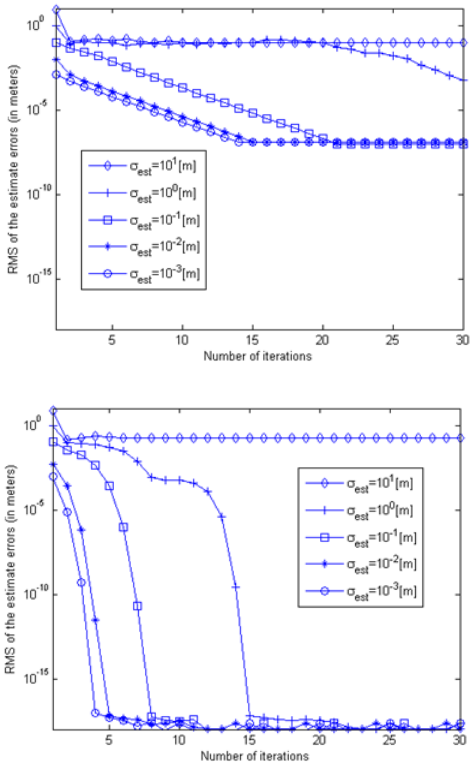


**Fig. 5.** Convergence comparison. The plots show the calibration accuracy of the ITE (top) and TAS (bottom) calibration approaches. The RMS of the ground-truth errors are plotted for different starting estimates. The standard deviation of the initial estimates is given in the legend (in meters). No measurement noise was assumed. The error RMS is on the vertical axis; the horizontal axis gives the number of iterations.

**Convergence analysis.** The typical size of the *region of convergence* was evaluated first. The initial estimate values were derived from the set of simulated ground truth positions and delay values by adding stochastic errors of various magnitudes; then the Gauss-Newton method (3) and (4) iterated 30 times. The calibration results (root-mean-square differences between the ground-truth positions and outcome of the calibration) for noiseless measurements can be seen in Fig. 5 for both the ITE and the TAS approaches. The convergence region is surprisingly large – in the magnitude of the diameter of the USCT system (20 cm), so in the absence of noise, a large error in the initial estimate is acceptable.

A rather large difference in the *speed of convergence* and in the *achieved accuracy* between the ITE and TAS approaches can be observed in Fig. 5. The TAS calibration approach (bottom graph) converges much faster than the ITE

approach (top graph). Also the achieved accuracy of the estimates is much better using the TAS approach.

With simulated noiseless TOA measurements, the accuracy of each calibration approach is limited only by the (im)precision of the used data type (Matlab's double-precision floating point). Still, the ITE approach cannot achieve accuracy better than about $10^{-7}$ [m]; on the other hand the TAS approach reaches accuracy of $10^{-18}$ [m] or better. The reason for this significant difference between the ITE and TAS approach is revealed by the condition number analysis.

**Condition number analysis.** The condition number of a matrix indicates the sensitivity of a linear equation system solution to errors in the data [13]. A condition number close to 1 indicates a well-conditioned system matrix and a "well-posed" problem. The higher the condition number, the more sensitive the solution is to noise in the data. For high condition numbers, the problem of solving the equation system becomes "ill-posed".

For the ITE calibration approach, the condition number is dependent on the transducer element positions. If the elements are rather randomly distributed in space, the position calibration is a well-conditioned problem. On the other hand, if – for example – all of the emitter transducers would lie in a line, the position calibration in the directions perpendicular to the line would be impossible, and the problem would be ill-posed. The cylindrical geometry of the USCT is unfortunately closer to the second case: if the transducer elements lie symmetrically on a perfect cylinder, the condition number is very high. The further we get from this perfect geometry, the lower the condition number gets, and the more well-posed the problem becomes. In contrast, the TAS approach doesn't show such a behavior. The condition number, although fairly high, stays virtually constant independently on the USCT cylindrical symmetry distortion.

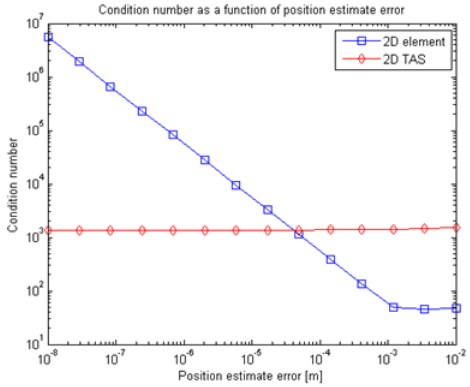


**Fig. 6.** Condition number as a function of position error.

To demonstrate this behavior, the condition number was calculated for different initial position error values for both the ITE and the TAS approaches. The initial position estimates were randomly distributed around the perfect cylindrical (ground truth) positions, with the typical magnitude of the estimate error ranging from one centimeter to one hundredth of a micrometer in random directions. For each error magnitude value, the initial position estimates were randomly generated one hundred times. Then the system matrix was set up and the condition number was calculated for each of those one hundred random realizations. A mean condition number versus initial error magnitude was then plotted in Fig. 6.

The above graph shows that in the ITE approach, the closer are the estimates to the actual transducer positions (lying on the perfect cylinder), the higher is the condition number. In each Gauss-Newton iteration, the position estimates are updated by calculating the estimate error. As this error gets smaller, the system matrix becomes more and more ill-conditioned. That is the main reason why the speed of convergence is slower than in the TAS approach, where the condition number stays constant.

**Noise effect analysis.** In the previous paragraphs we examined the behavior of both calibration approaches in absence of measurement noise or inaccuracies. Such noise, however, must be expected in a real USCT setup especially in the measurement of the time-of-arrival of a pulse.

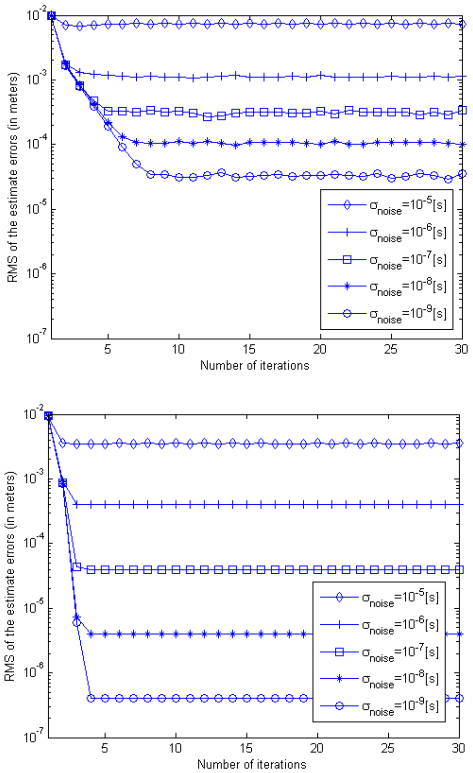


**Fig. 7.** Noise effects analysis for the ITE (top) and TAS (bottom) approaches. The two plots show the calibration accuracy (median RMS of the estimate errors) for different levels (standard deviations) of measurement noise (pulse detection inaccuracies) versus number of iterations. The typical error of the initial estimate was set to $10^{-2}$ m.

The recorded A-scan, in which the pulse is being detected, is itself noisy due to imperfections of the used equipment. This A-scan noise complicates determining the TOA of a pulse precisely. Moreover, the pulse detection algorithm is also inaccurate to a certain extent. Also the speed of sound, calculated from the measured temperature of the water in the USCT tank, is not exact. Besides the inaccuracies of the thermometer and the error of the formula to calculate the speed of sound from the measured temperature, the temperature inside the tank is not fully homogeneous.

All these sources of error cause that the calibration method performs somewhat worse than under ideal conditions. The following paragraphs analyze how both the calibration approaches perform in simulated noisy conditions.

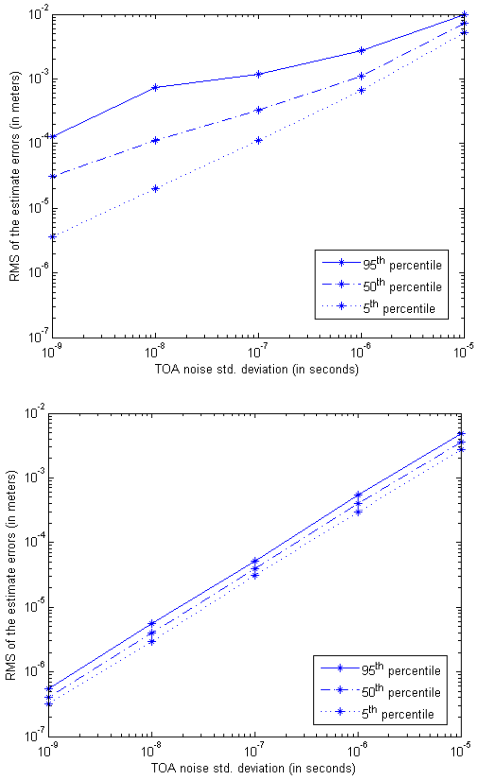


**Fig. 8.** Dependency of the calibration accuracy on the TOA noise strength for the ITE (top) and TAS (bottom) approaches.

To evaluate how the calibration method performs in presence of noise, the same mathematical model was used as for the convergence analysis. The time-of-arrivals of the simulated pulses were calculated according to (1) for each emitter-receiver pair. Normally distributed random noise with a preset standard deviation was added to the simulated TOA values. The initial position and delay estimates were again randomly distributed around the ground truth values.

To see the effect of the noise level on the calibration method, the standard deviation of the TOA noise was preset to 5 values ranging from $\sigma_{noise} = 10^{-9}$ s to $\sigma_{noise} = 10^{-5}$ s. The calibration process ran 100 times (with 100 stochastically diversified input data) for each of these preset $\sigma_{noise}$ values.

The results – median RMS values of calibration errors versus number of iterations - can be seen in Fig. 7 for both the ITE and TAS calibration approaches. As one can see, the TAS approach performs much better: it converges faster to estimates which are closer to the ground truth.

To show the dependency of the calibration accuracy on the TOA noise level, a pair of graphs were plotted in Fig. 8. The solid lines show the 95$^{\text{th}}$ percentile of the estimate error RMS values after the calibration. They therefore show the expected 95 % accuracy of the calibration results in the presence of noise. It can be seen that in order to satisfy the needs of the USCT image reconstruction requiring transducer position accuracy within a tenth of a millimeter, the pulses must be detected with an error under $10^{-9}$ s for the ITE approach which is not practically achievable as it corresponds to about 0.003 of the period (at 2.7 MHz). On the other hand, for the TAS approach it is sufficient to detect pulses within $2 \cdot 10^{-7}$ s, i.e. about 2/3 of the period of the used ultrasound. This precision is more likely achievable in the current USCT setup.

# 4. Experimental Verification

The described method was utilized for calibration of the experimental 3D USCT system Model I in the Forschungszentrum Karlsruhe (KIT) Germany, in the following way: A so called empty measurement was performed with the USCT tank filled with pure degassed water, providing raw US signals – A-scans – for all combinations of emitters and receivers. Because the full 3D scan of data in the USCT system takes a long time, during which the water temperature may change in a non-negligible extent due to disseminated US power, the temperature was measured – and the speed of sound was calculated – in 5 minute intervals. The real instantaneous temperature-dependent speed of sound was calculated using the Marczak algorithm [14]. To compensate in the following calculations for the temperature changes, all the affected terms in one row of the Jacobian (6) (corresponding to a particular A-scan) were calculated using the interpolated value of the sound speed determined by the time the A-scan was taken at.

In the RF signal data provided by the USCT measurement, the times of arrival (TOAs) were detected in the recorded A-scans using a set of filters and basically identifying the maximum of the filtered transmission pulses. Detailed description of the detection approach, the temporal accuracy of which is crucial, is out of scope of this paper. It should be noted that the presented calibration method is independent on the method of extracting the TOAs, so that other approaches, as e.g. cross-correlation (matched filtering) or detection methods based on transforms can be used if more appropriate under different conditions. The obtained TOAs constituted the input to the optimisation procedure.

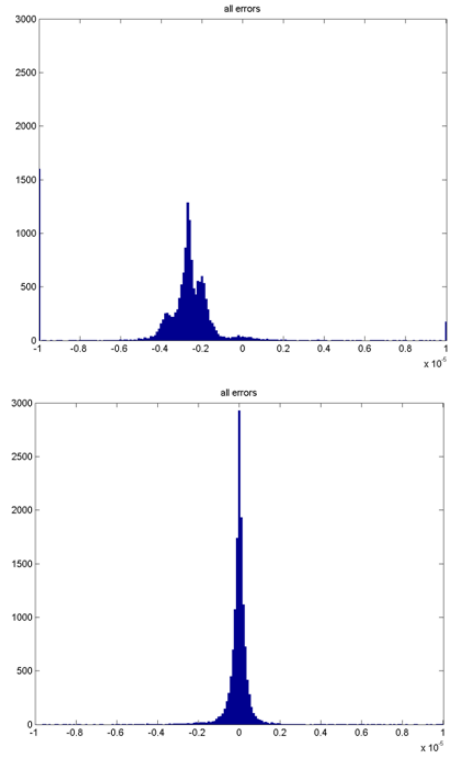


**Fig. 9.** Histogram of TOA errors before (top) and after (bottom) the calibration.

To start the optimising iteration, the initial estimated values were chosen as follows: The initial estimate of the transducer positions was taken from the mechanical design documents of the USCT system, particularly of the cylindrical steel frame, on which the TASes are mounted, and which forms the outer shape of the USCT tank, and also from technical drawings of the TASes. The time-delays of all transducers, as further parameters to be determined by the optimisation, were all set to zero in the initial estimate. The iterative optimisation was then run; both above described approaches to calibration were practically tested, with largely different results. The calibration using the individual transducer (ITE) approach did not converge in a reasonable number of iteration steps, whereas the transducer array (TAS) based approach did converge well, yielding the calibrated transducer positions, which were well acceptable considering the possible mechanical tolerances of the USCT system; also the calculated transducer delays were in a reasonable range. Unfortunately, there are no means how to verify directly the accuracy of the calibration results, as the ground truth is not measurable: physical measurements of distances are not feasible, primarily due to inaccessibility of the transducers inside the system by a gauge of the required precision, and also due to enormous amount of the needed measurements (i.e. combinations of transmitter – receiver). This also prevents any systematic direct measurements of the transducer delays. Under this situation, the only way how to evaluate the calibration consistency is indirect, i.e. to use the calibration results for modifying (correcting) accordingly the measured TOAs and make conclusions based on the subsequent results influenced or determined by TOAs.

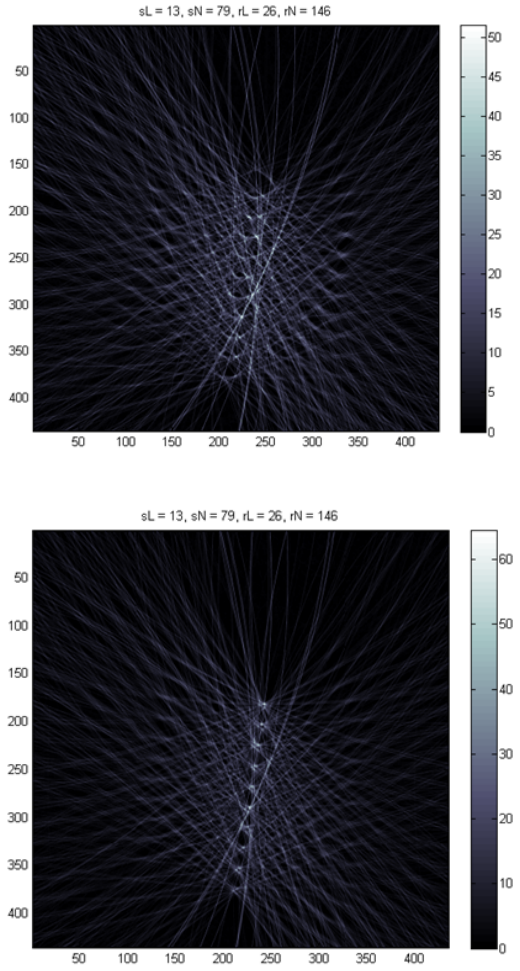


**Fig. 10.** Reconstructed reflectivity images of a thread phantom before (top) and after (bottom) the calibration.

As a test of consistency, the corrected TOAs have been statistically evaluated with rather convincing results, as follows. In the lack of ground truth, the measured TOAs (both corrected and uncorrected) can only be compared with the values (CTOAs in eq. (5)), computationally obtained from the supposed ideal geometry of the system; the differences being considered TOA errors for each individual A-scan (i.e. each emitter-receiver link). These errors are the elements of the residual vector (5) and thus would ideally be all zero after the calibration (i.e. the histogram would have a single column at zero of TOA error axis), while errors are generally nonzero for non-calibrated TOAs due to mechanical imprecisions in the system manufacture. Fig. 9 shows histograms of the TOA errors before (upper panel) and after calibration (lower panel). Before the calibration, the histogram has its maximum at a non-zero TOA error, i.e. with uncalibrated transducer positions and time-delays most of the TOAs are below expectations. Also, the variance of errors is fairly large. On the contrary, the histogram after the calibration shows only a narrow peak centered at zero error and the variance is clearly smaller, which indicates that the transducer positions and delay parameters were reasonably calibrated thus minimizing the overall measurement error.

Another, more demanding test, more oriented to the ultimate aim of imaging, consist in comparing the properties of tomographic images obtained from the same USCT measurement data set, but with and without corrections based on the calibration. This enables to assess the influence of the calibration on the quality of final reconstructed images. Such an experiment has been designed and realized using a phantom of a difficult object (from the imaging point of view), which at the same time allows easy visual appraisal of the imaging quality. The phantom consisted of 10 parallel threads in a vertical plane, of 0.5 mm diameter each (less than the US wavelength), stretched vertically inside the USCT tank. The horizontal slice of the reconstructed image data should then ideally contain – thanks to small transverse dimension of threads – ten point objects along a straight line. Using the non-calibrated and calibrated data, the image of the thread phantom was reconstructed from otherwise identical measurement data. Fig. 10 compares the respective reconstructed image slices (2D horizontal cross-sections of the threads) from non-calibrated (upper figure) and calibrated (lower figure) data. Due to the highly demanding object, both images suffer with star artefacts from the reconstruction algorithm that are inherent to this type of imaging, however, the peaks indicating the threads positions are substantially better defined below, indicating a substantial improvement in minimizing the size of the point-spread-function (PSF) of the imaging thus a much better spatial resolution. Although it is not obvious from the images, the artifacts are relatively weaker in the lower image thanks to better focusing.

Based on both tests, it can be concluded that the calibration brought a significant improvement in focusing the image and even relatively suppressing the artifacts.

# 5. Conclusions

A novel method was developed for the calibration of a USCT system using the so called empty measurement with following numerical nonlinear optimisation to determine the corrections of transducer positions and time delays. The paper formulates the principle of the method, which generalises the idea of GPS. The main extension over the GPS approach is that neither the emitter nor the receiver positions are assumed to be known (therefore it does not require a reference coordinate frame) and all transducer parameters are calibrated simultaneously, including the a-priori unknown individual signal delays in the transducers. The paper introduces two versions of the method: the ITE approach calibrating individual positions and delays of the ultrasonic transducer elements, and the TAS approach calibrating the positions and orientations of transducer-array-systems (groups of the transducer elements), including the delays. Both approaches underwent a thorough simulation analysis, which has proved both good convergence properties and robustness with respect to measurement noise. The accuracy of the USCT system calibration based on real US signals is crucially dependent on the precision of the pulse arrival detection in the signal; this is a problem concerning the concrete application of the method and is treated separately. The calibration is self-contained – no calibration phantoms, high precision positioning devices, etc., are needed, and the calibration can easily be repeated when required.

Practical experiments have shown that the measurements taken on the current USCT system are sufficient for a TAS approach based calibration, when sophisticated pulse detection methods are used. In contrast, the ITE approach, although theoretically also correct, has failed with real signals due to generally higher sensitivity to the measurement noise. The experiment, comparing the results of image reconstructions based on non-calibrated and calibrated data, confirmed the utility of the calibration and indicates an important potential for improvement of imaging properties of the USCT modality.

The continuing research should be aimed at routine application of the calibration procedure, which might be supported by continuing development of the so far experimental imaging system. In parallel, there is an intensive research of the system hardware (a new generation of non-cylindrical systems) and data acquisition procedures, and also of the reconstruction algorithms; both may be expected to bring impulses for further development of the described calibration method.

# Acknowledgements

Authors sincerely acknowledge the contribution of Dr. Rainer Stotzka and Dr. Nicole Ruiter, the authors of the experimental USCT system, both of the Forschungszentrum Karlsruhe Germany (KIT).

This project has been sponsored by the research centre DAR (Ministry of Education, Czech Republic, project no. 1M0572), by the DAAD grant no. D12-CZ9/07-08, and partially also by the research frame of the FEEC BUT (Ministry of Education, Czech Rep., project no. MSM 0021630513).

# References

[1] RUITER, N. V., SCHWARZENBERG, G. F., ZAPF, M., LIU, R., STOTZKA, R., GEMMEKE, H. 2J-2 3D ultrasound computer tomography: Results with a clinical breast phantom, In *IEEE Symposium on Ultrasonics*. Vancouver (Canada), 2006, p. 989 - 992.

[2] JIŘÍK, R., STOTZKA, R., TAXT, T. Ultrasonic attenuation tomography based on log-spectrum analysis. In *Medical Imaging 2005: Ultrasonic Imaging and Signal Processing*. San Diego (CA, USA), 2005.

[3] STOTZKA, R., et al. *A New 3D Ultrasound Computer Tomography Demonstration System*. [Online] Forschungszentrum Karlsruhe, 2004. Available at: www.stotzka.de/Publications/stotzka2004.3.html

[4] YUE L. Position and time-delay calibration of transducer elements in a sparse array for underwater ultrasound imaging. *IEEE Transactions on Ultrasonics, Feroelectrics, and Frequency Control,* 2006, vol. 53, no. 8, p. 1458 - 1467.

[5] COX, T. F., COX, M. M. *Multidimensional scaling*. London (UK): Chapman Hall, 1994.

[6] BIRCHFIELD, S. T., SUBRAMANYA, A. Microphone array position calibration by basis-point classical multidimensional scaling. *IEEE Transactions on Speech and Audio Processing*, 2005, vol. 13, no. 5, p. 1025 - 1034.

[7] FILIPIK, A., PETERLIK, I., HEMZAL, D., JAN, J., JIRIK, R., ZAPF, M., RUITER, N. Calibrating an ultrasonic computed tomography system using a time-of-flight based positioning algorithm. In *29th Annual International Conference of the IEEE Engineering in Medicine and Biology Society EMBS 2007.* Lyon (France), 2007, p. 2146 - 2149.

[8] FILIPIK, A., JAN, J., PETERLIK, I., HEMZAL, D., RUITER, N., JIRIK, R. Modified time-of-flight based calibration approach for ultrasonic computed tomography. In *30th Annual International Conference of the IEEE Engineering in Medicine and Biology Society EMBS 2008.* Vancouver (Canada), 2008, p. 2181 - 2184.

[9] HOFMANN-WELLENHOF, B., LICHTENEGGER, H., COLLINS, J. *GPS: Theory and Practice*. Vienna (Austria): Springer-Verlag, 2001.

[10] HILL, C. R., BAMBER J. C., HAAR, G. R. *Physical Principles of Medical Ultrasonics*, 2nd Ed. New York (USA): Wiley, 2004.

[11] PRESS, W. H., FLANNERY B. P., TEUKOLSKY S. A., VETTERLING W. T. *Numerical Recipes in C: The Art of Scientific Computing.* 2nd Ed. Cambridge (UK): Cambridge University Press, 2002.

[12] CRAIG, J. J. *Introduction to Robotics: Mechanics and Control.* Reading (MA, USA): Addison-Wesley, 1989.

[13] ASTER, R. C., THUBBER, C. H., BORCHERS, B. *Parameter Estimation and Inverse Problems*. Burlington (MA, USA): Elsevier Academic Press, 2005.

[14] MARCZAK, W. Water as a standard in the measurements of speed of sound in liquids. *The Journal of the Acoustical Society of America*, 1997, vol. 102, no. 5, p. 2776 - 2779.

## About Authors...

**Adam FILIPÍK**, MSEE, PhD, graduated at Brno University of Technology in biomedical engineering (2003) and then remained at the Dept. of Biomedical Engineering as a doctoral student (2003 – 2007). He obtained his PhD in biomedical electronics and biocybernetics in 2008. He participated on a research project concerning 3D freehand ultrasonography (2003 – 2004) and between 2005 and 2007 he was a member of Brno group of the research center DAR (Data, Algorithms and Decision making), working primarily on problems of ultrasonic 3D transmission computed tomography (USCT). Since then he is employed by an international industrial company.

**Jiří JAN**, MSEE and PhD in radioelectronics, Associate Professor (1978), Full Professor (1991) at Brno University of Technology (Czech Republic). During his professional life, he served here and abroad as a university teacher and researcher, initially oriented at digital analysis of antennas and electromagnetic wave propagation. In 1980ties he turned his interest to digital signal processing and later also to image processing and analysis, particularly (but not exclusively) in biomedical engineering applications. Between 1990 and 2010 he headed the Department of Biomedical Engineering, FEEC, Brno UT, where he formulated the present concept of study of Biomedical and ecological engineering; presently he is a full Professor of biomedical signal and image processing at the Department. Since 1978 till 2010 he was chairing the international programme committee of the biennial international conference BIOSIGNAL supported by EURASIP and IEEE - EMBS. He has published two book monographs: J. Jan: Medical Image Processing, Reconstruction and Restoration; Concepts and Methods (CRC Taylor & Francis, New York: 2006, 730 pp,) and J. Jan: Digital Signal Filtering, Analysis and Restoration (IEE Press, London: 2000, 407 pp.), and over 240 conference and journal papers. He was or is serving as Associate Editor for IEEE-Trans. on Biomedical Engineering (IEEE, 1996-2001), for J. on Advances in Signal Processing (EURASIP – Springer, since 2000) and others, and as a regular reviewer of numerous scientific journals. His present research interests are in the area of medical image data processing, concerning namely multimodal image fusion, diagnostic feature analysis and image reconstruction from non-image data.

**Igor PETERLÍK** MSc, PhD in computer science, graduated in informatics and after doctoral study received his PhD degree in the same area from the Masaryk University, Czech Republic (2009). From 2005 to 2009, he worked as a member of Brno group of the research center DAR (Data-Algorithms-Decision making) coordinated by the Academy of Sciences of the Czech Republic. In 2009 he joined INRIA Lille Nord-Europe in France where he participated in the European project PASSPORT (PAtient Specific Simulation and PreOperative Realistic Training for liver surgery) as a post-doctoral fellow. In 2011 he started a post-doctoral fellowship at the University of British Columbia, Vancouver, Canada. His research interests include medical simulations, computer haptics, image reconstruction, numerical methods, parallel and distributed computing.